Applied Catalysis B: Environmental 188 (2016) 98–105

Contents lists available at ScienceDirect

Applied Catalysis B: Environmental

journal homepage: www.elsevier.com/locate/apcatb

Occurrence of radical and nonradical pathways from carbocatalysts for aqueous and nonaqueous catalytic oxidation

Xiaoguang Duan[a], Zhimin Ao[b], Li Zhou[a], Hongqi Sun[a,*], Guoxiu Wang[b], Shaobin Wang[a,*]

[a] Department of Chemical Engineering, Curtin University, GPO Box U1987, WA 6845, Australia
[b] Centre for Clean Energy Technology, School of Mathematical and Physical Sciences, University of Technology Sydney, PO Box 123, Broadway, Sydney, NSW 2007, Australia

ARTICLE INFO

Article history:
Received 1 December 2015
Received in revised form 20 January 2016
Accepted 25 January 2016
Available online 28 January 2016

Keywords:
Nonradical oxidation
Radical scavenger
Peroxymonosulfate activation
DFT
Carbocatalysis

ABSTRACT

Metal-free activation of superoxides provides an efficient and environmentally benign strategy for heterogeneous catalytic oxidation. In this study, nanocarbons with varying carbon-conjugation structures and functional groups were investigated for peroxymonosulfate (PMS) activation. It was discovered that radical and nonradical oxidations could occur on different carbocatalysts depending on the carbon structure. Radical oxidation occurs exclusively on MWCNTs and CMK-3, similar to a metal oxide, MnO_2. Both radical and nonradical oxidations are very pronounced in nanodiamond (AND-900)/PMS whilst nonradical oxidation is dominated in reduced graphene oxide (rGO-900)/PMS. Density functional theory (DFT) calculations were employed to explore the PMS adsorption and O—O bond activation on the different carbon configurations for an in-depth probe of the activation mechanism. The intact sp^2-conjugated π system in MWCNTs and electron-rich ketonic groups (as Lewis basic sites) in CMK-3 can stimulate PMS dissociation to generate $SO_4^{\bullet-}$ and $^{\bullet}OH$, similar to metal-based catalysts. However, the defective edges at the boundary of carbon network are able to facilitate the organic degradation without generation of the reactive radicals, which is well supported by both experiments and the DFT calculation. The emerging nonradical oxidation induced by the carbocatalysis is superior to the radical oxidation on most metal oxides for effective degradation of various organics. The influences of solution pH, various anions ($H_2PO_4^{2-}$, HCO_3^- and Cl^-) and background organic matters (humic acid) on the nonradical oxidation were further evaluated. The nonradical oxidation on carbocatalysts can be utilized as a green and effective oxidation strategy for aqueous environmental remediation and nonaqueous phase oxidation.

1. Introduction

The environmental deterioration, coming along with the industrialization and civilization of our modern society, has triggered worldwide concerns on the detrimental aspects to a sustainable future. Considerable efforts have been made to utilize the state-of-the-art technologies such as physical adsorption, flocculation/coagulation, photocatalysis, bio-degradation, and chemical oxidation for remediation of the contaminated atmosphere, waterbody, and soil in the eco-system [1–4]. Advanced oxidative processes (AOPs) are most widely used for decomposition of toxic organic contaminants in wastewater into harmless mineral acids, carbon dioxide and water, taking advantage of the reactive species from activated superoxides. For instance, Fenton reactions are based on a homogeneous Fe^{2+}/H_2O_2 system to produce hydroxyl radicals ($^{\bullet}OH$) which attain the destruction of a wide range of organic contaminants in aqueous solutions [5,6]. However, Fenton reaction requires stoichiometric dosages of the oxidant (H_2O_2) and ferrous salts, both are chemically unstable resulting in intensive inputs for transportation, storage and handling [7]. The reaction is also restricted by metal catalysts, strict reaction environment (pH < 3), generation and coagulation of sludge [8,9].

Sulfate radicals ($SO_4^{\bullet-}$), produced from peroxysulfate salts, have demonstrated a great capability of attacking organics via electron and hydrogen abstraction/addition, similar to hydroxyl radicals [10,11]. Moreover, sulfate radicals possess a higher standard reduction potential and present more selective degradation of organics with unsaturated bond and aromatic structure especially at neutral conditions [12–15]. As a typical peroxysulfate

* Corresponding authors.
E-mail addresses: h.sun@curtin.edu.au (H. Sun), shaobin.wang@curtin.edu.au, wangshao@vesta.curtin.edu.au (S. Wang).

http://dx.doi.org/10.1016/j.apcatb.2016.01.059
0926-3373/

salt, peroxymonosulfate (PMS, also known as oxone) with an asymmetric structure (HO–SO_4^-) can be activated by various transition-metal ions and metal oxides to generate both $SO_4^{\bullet-}$ and $^{\bullet}OH$ [16–18]. The variable chemical states and unoccupied orbitals of the metal-based catalysts are believed to enable the electron transfer in a redox cycle to activate PMS molecules to produce the reactive radicals.

More recently, as promising alternatives in terms of green remediation technologies, nanocarbons such as graphene and carbon nanotubes were discovered to be able to effectively activate PMS to produce free radicals [19,20]. The eco-friendly and metal-free nature of the nanocarbons with ultrahigh pore volumes and specific surface areas (SSAs) can serve as excellent candidates for adsorption and carbocatalysis in environmental remediation, completely preventing the toxic metal ion leaching even in a strong acid or alkaline environment. Distinct from the metal oxides with exposed facets and valence states, most of the carbocatalysts are constructed with various defects, heteroatoms doping, functional groups, and carbon configurations, making it more difficult to investigate and identify the intrinsic active sites accounting for carbocatalysis [21,22]. It is believed that different active sites may play unique roles in heterogeneous catalysis due to the characteristically chemical states, reactive potential, and binding structure with the reactants.

Previously, Fenton or Fenton-like reaction was believed to be exclusively radical-based oxidation. However, few recent investigations suggested that nonradical reactions may occur for some catalyst systems. The nonradical processes were first revealed in a homogeneously selective hydrocarbon activation in which transition metal ions (Fe^{III} or Ru^{III}) were able to interact with H_2O_2 to form metal-oxo ($Fe^{V}=O$ or $[Ru_3{}^{IV,IV,III}=O]^+$) species as active intermediates to facilitate the cleavage of C—H bond and promote the catalytic oxidation without radical generation [23,24]. Croué and co-workers discovered a copper oxide (CuO) can effectively activate ozone (O_3) and persulfate (PS) for contaminant degradation with an outer-sphere electron-transfer mechanism [25,26]. N-Doping on highly crystallized single-walled carbon nanotubes could also induce the nonradical oxidation with PMS [27]. However, little has been reported in nonradical reaction in pristine carbocatalysts.

In this study, we investigated diverse nanocarbons in different dimensions, carbon types, and functional groups to reveal the pristine carbocatalysis in an aqueous-phase catalytic oxidation of various organic compounds such as dyes, phenolics, and antibiotics. The nonradical oxidation was for the first time discovered on reduced graphene oxide and annealed nanodiamond. The defective edges are believed to be the active sites to mediate the novel oxidation pathway. We also employed DFT calculations for theoretical understandings of the occurrence of the nonradical mechanism. Moreover, versatile environmental implications of inorganic anions, halogen, and background organic matters in water were estimated in the emerging nonradical reaction induced by carbocatalysis. We dedicate this work to proposing a novel and effective technology of oxidative catalysis for organic degradation and green remediation, which can be used in both aqueous and nonaqueous oxidations.

2. Experimental

2.1. Materials and preparation

The simulated pollutants and chemicals such as phenol (≥99.5 wt.%), methylene blue (dye content ≥82 wt.%), 1,2-dihydroxylphenol (≥99.0 wt.%), sulfachloropyridazine (analytical standard), and humic acid (inorganic residue ~20 wt.%) were obtained from Sigma-Aldrich, Australia. Multi-walled carbon nanotubes (MWCNTs, OD 10–20 nm, length 30 μm, purity >95 wt.%) were purchased from Timesnano, China. A cubic-ordered mesoporous carbon (CMK-3, specific surface area (SSA) >900 m^2/g, pore volume 1.2–1.5 cm^3/g, pore diameter 3.4–4 nm) was obtained from XF NANO, China. Diamond nanopowders (particle size <10 nm (TEM), bulk density 0.2–0.7 g/mL) were obtained from Sigma-Aldrich, Australia. Annealed nanodiamonds were obtained by treating the pristine samples in a tubular furnace under nitrogen atmosphere at 900 °C for 1 h (denoted as AND-900) at a heating rate of 5 °C/min. Graphene oxide (GO) was prepared via a modified Hummers' approach [28]. Reduced graphene oxide (rGO) was prepared via the same thermal treatment as AND-900 and labelled as rGO-900. The detailed procedure for preparation of several metal oxides can be found in previous studies [26,29,30].

2.2. Characterization of carbocatalysts

Transmission electron microscopy (TEM) was conducted on a JEOL JEM-2100F instrument operating at 200 kV and the images are shown in Fig. S1. The rGO-900 presents as folded sheets with a silky-smooth morphology, whereas the AND-900 is randomly stacked together with a characteristic core/shell structure. CMK-3 has a structure of well-ordered porous layers. The crystalline structures (Fig. S2) of the carbocatalysts were recorded on an X-ray diffraction (XRD) instrument (Bruker D8 Advance) under a filtered Cu-Kα radiation at λ = 1.5418 Å. The great peak at 2θ = 26.3° of rGO-900 and MWCNT is corresponding to the (002) facet of the sp^2-hybridized graphitic carbon network, while the peak at 2θ = 42.0° of AND-900 can be ascribed to the sp^3-bonded diamond core with a d-spacing of 2.1 Å. The disorder degree of carbon materials was reflected in Raman spectra (Fig. S3), acquired from an argon ion laser equipped ISA laser Raman instrument at 514 nm. The intensity ratios (I_D/I_G) of rGO-900, MWCNTs, and CMK-3 were estimated to be 1.70, 1.35, and 1.17, respectively, suggesting the different degrees of heteroatoms doping and defective sites (edges and vacancies). The surface graphitic curvatures of annealed nanodiamonds are well reported to possess various surface defects with ill-defined structures [31,32]. The thermal behavior of the nanocarbons was recorded on a Mettler–Toledo–Star instrument under air atmosphere at a heating rate of 5 °C/min from 35 to 900 °C (Fig. S4). Annealed nanodiamonds presented a better thermal stability owing to the robust core structure. Surface functional groups of the carbocatalysts were analyzed by a Fourier-transform infrared (FTIR) spectroscopy (Fig. S5) on a PerkinElmer instrument. Most of the functional groups on rGO-900 and AND-900 were removed after the thermal annealing. The specific surface areas (SSAs) and pore structure of the nanocarbons were obtained on a TriStar II equipment and estimated by the Brunauer–Emmett–Teller (BET) equation and Barrett-Joyner-Halenda (BJH) method, respectively (Fig. S6). CMK-3 presents the largest SSA and pore volume due to the well-ordered mesoporous structure. X-ray photoelectron spectroscopy (XPS) was utilized to probe the surface compositional information under an Al-Kα X-ray radiation. All XPS spectra (Fig. S7 and Fig. S8) were calibrated with C1s at 284.5 eV and analyzed with CasaXPS software. The oxygen contents decreased from 32.0 at% (GO) to 6.0 at% (rGO-900) owing to the removal of oxygen functional groups during the heat treatment. The oxygen level of nanodiamond slightly dropped from 5.7 at% (ND) to 3.7 at% (AND-900). The structure and chemical properties of the carbocatalysts are summarized in Table S1.

2.3. Experimental procedure

The as-made metal-free catalysts were evaluated for catalytic oxidation of organics with PMS. A 20 ppm phenol solution was prepared from a 1000 ppm phenol stock solution with a pH of

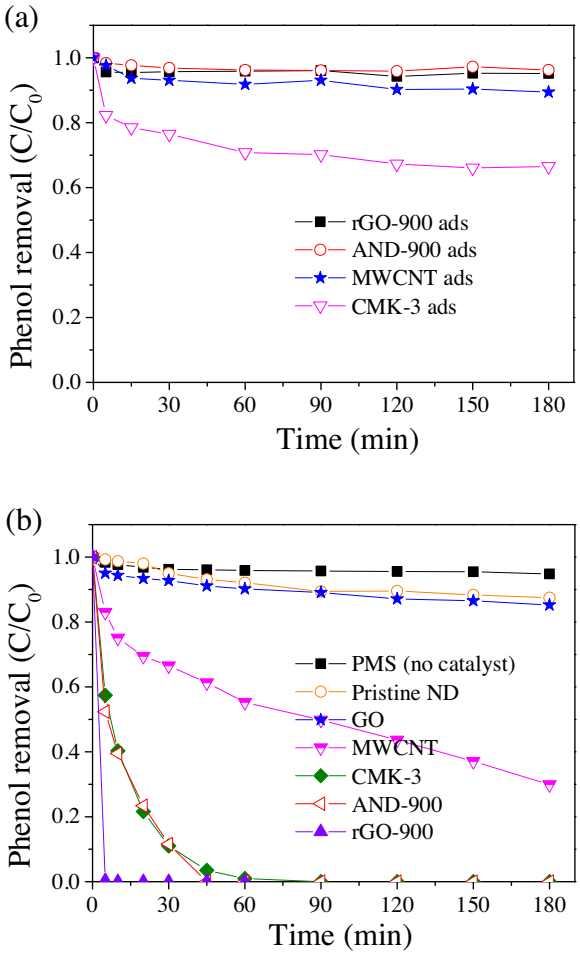

Fig. 1. (a) Phenol adsorption on nanocarbons, (b) phenol oxidation by PMS activation on nanocarbons. ([Catalyst]$_0$ = 0.1 g/L, [PMS]$_0$ = 6.5 mM, [T] = 25 °C, and [Phenol]$_0$ = 20 mg/L).

5.9 ± 0.1 without any buffering. During the reactions, the solutions were withdrawn and filtered by 0.45 μm PEFT membrane filters and then immediately mixed with methanol solution to scavenge the reactive species and terminate the oxidation. The mixture was then analyzed on an ultrahigh performance LC system (UHPLC, UltiMate® 3000). Catechol and phenol were evaluated with a HPLC Acclaim OA column and an UV detector set at 270 and 290 nm, respectively. Sulfachloropyridazine (SCP) was determined with a RSLC C18 column and an UV detector set at 270 nm. A UV–vis spectrophotometer was utilized to measure the concentration of methylene blue (MB) at 664 nm. For evaluation of the radical quenching effects, certain amounts of a radical scavenger (methanol, calibrated by molar ratio MeOH/PMS) were introduced into the reactions to quench the reactive radicals.

3. Results and discussion

3.1. Adsorption and catalytic oxidation of phenolics on nanocarbons

The adsorption capabilities of the nanocarbons are indicated in Fig. 1a. The mesoporous carbon (CMK-3) was able to remove 33.5% phenol, while reduced graphene oxide (rGO-900), annealed nanodiamond (AND-900) and multi-walled carbon nanotubes (MWCNTs) exhibited insignificant adsorption, providing phenol removal efficiencies at 4.9%, 3.8% and 10.6%, respectively. The superb adsorption capability of the CMK-3 is due to the porous structure with an extremely large pore volume and SSA. The effectiveness of phenol degradation/transformation by activating PMS on the nanocarbons is shown in Fig. 1b. PMS alone presents a very low efficiency for phenol oxidation. Pristine nanodiamond (ND) and graphene oxide cannot effectively activate PMS either. It is interesting to observe that MWCNTs and CMK-3 are able to achieve 70.1% and 100% phenol degradation in 3 h. After thermal annealing, the activities of AND-900 and rGO-900 are remarkably enhanced providing complete phenol removal in just 45 and 10 min, respectively.

To further exclude the implications of trace metal/metal oxide residues, the as-made carbocatalysts were thoroughly refluxed in hydrochloric acid (HCl). In the control tests on the acid-digested catalysts, negligible effect was observed as indicated in Fig. S9, suggesting that the intrinsic activity for PMS activation can be attributed to the pristine carbocatalysis. It can be seen that the catalytic activity of carbocatalysts cannot be solely correlated to the SSA or phenol adsorption capability but the specific active sites. Distinct from transition metal catalysts with variable chemical states and versatile oxygen bonding, the sp^2- hybridized carbon network with conjugated π systems is able to interact and weaken asymmetric O—O bond in PMS molecules (HO-SO_4^-), herein activating the PMS for oxidative reactions [33,34]. The active sites, such as kenotic groups working as Lewis basic sites and defective edges with certain metal-like behaviors in carbocatalysts, can further enhance the PMS activation process [19,20]. In this study, it is interesting to find that the catalytic performances of the nanocarbons for PMS activation are dramatically different. MWCNTs with an intact graphitic structure (I_D/I_G = 1.35) shows the lowest activity, whereas CMK-3 with a porous structure and various functional groups are more active. It is also noteworthy that pristine nanodiamond and GO are inert for PMS activation, and the activities are drastically boosted on AND-900 and rGO-900. The heat treatment is able to remove the coverage of disordered carbon and enable the formation of a multi-walled, onion-like structure due to the collapse and transformation from the surface sp^3-hybridized diamond core. Thus, the graphitic layers of AND-900 with curved shells and various defects are of a high chemical activity and present greater potential for redox reactions, compared with pristine nanodiamond [32,35]. Besides, the enhanced catalytic performance of rGO-900 can be ascribed to the removal of superabundant oxygen-functional groups, attaining better reducibility for electron conduction and releasing the defective edges occupied by the excess oxygen groups [19,29,36].

3.2. Radical and emerging nonradical oxidations

The carbocatalysts in this study are constructed with different carbon configurations, functional groups and defective sites. Therefore, it is of great importance to probe if each active site plays a different role in carbocatalysis for heterogeneous activation of PMS. Radical quenching reaction was applied to investigate the effect of reactive radicals in PMS/carbocatalyst systems. Varying amounts of methanol (MeOH) were introduced into the mixed solution to quickly eliminate both sulfate radicals ($k_{SO4}^{\bullet -}$ = 3.2 × 10^6 M^{-1} s^{-1}) and hydroxyl radicals ($k^{\bullet}_{OH}$ = 9.7 × 10^8 M^{-1} s^{-1}) [37]. As indicated in Fig. 2, the carbocatalysts presented totally different performances for catalytic oxidation of phenol in the presence of methanol. The phenol oxidation efficiency on MWCNTs sharply decreased to 13.5% from 70.2% at a ratio of 500:1 (methanol: PMS) (Fig. 2a). The oxidation reaction was completely terminated at the ratio of 1000:1. For comparison, the reaction rate went down gradually when MeOH was added into CMK-3/PMS (Fig. 2b) or AND-900/PMS (Fig. 2c). When the solvent of water was completely replaced by MeOH (with only 1% water remaining introduced from the phenol solution), the oxidation reaction completely

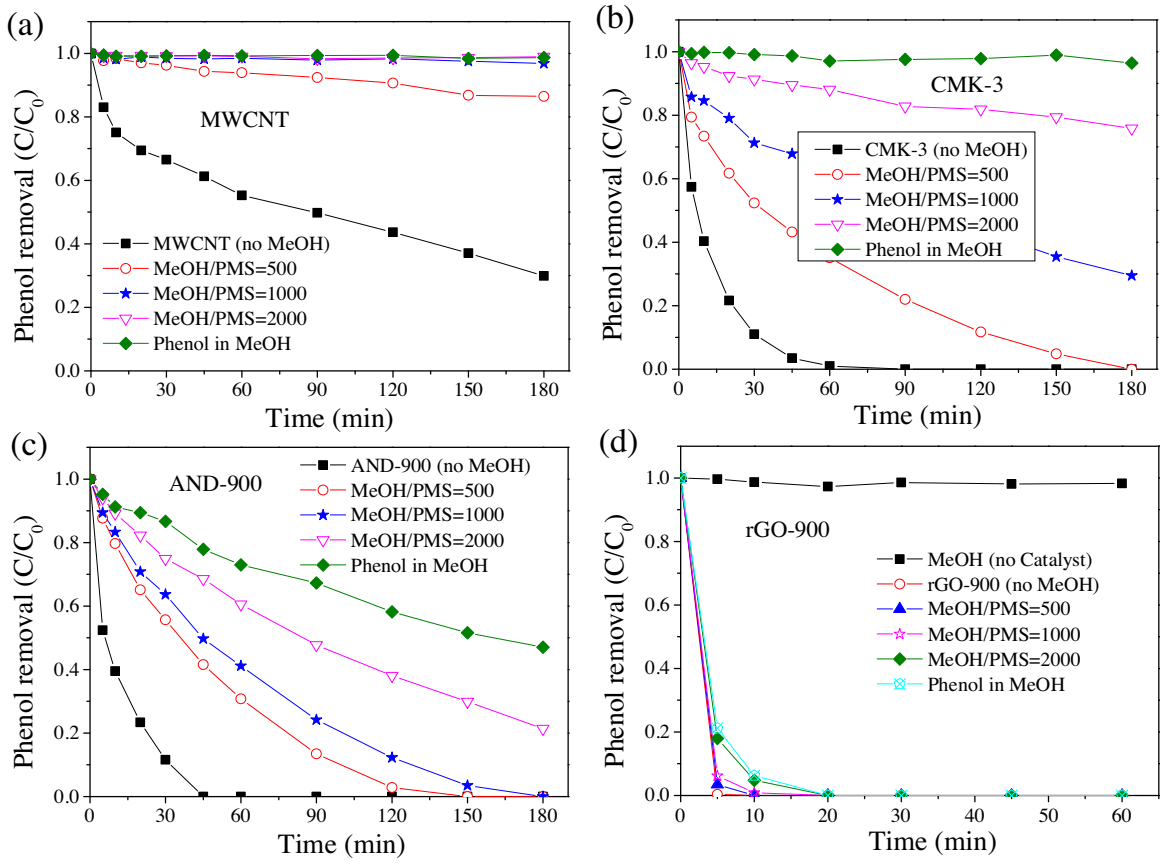

Fig. 2. Effect of methanol quenching on phenol oxidation on (a) MWCNTs, (b) CMK-3, (c) AND-900, and (d) rGO-900. ([Catalyst]$_0$ = 0.1 g/L, [PMS]$_0$ = 6.5 mM, [T] = 25 °C, and [Phenol]$_0$ = 20 mg/L).

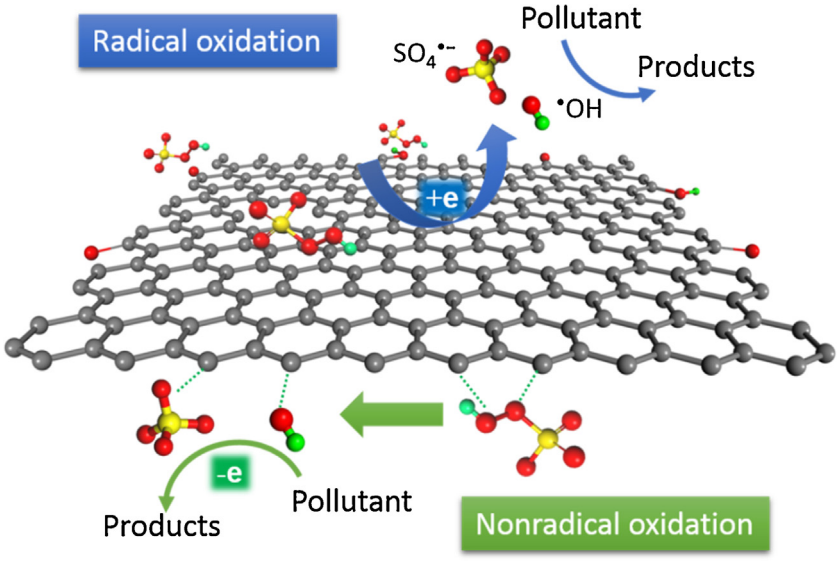

Scheme 1. Mechanism of PMS activation on carbocatalysts.

disappeared in CMK-3/PMS while 52.9% phenol degradation was still achieved in AND-900/PMS. In addition, the impact of MeOH on rGO-900/PMS was almost negligible and a stunning 100% phenol removal was still achieved in just 20 min in MeOH solution (Fig. 2d). The initial reaction rate constants of the catalysts under different concentrations of MeOH were displayed in Table S2. The reaction rate constants decreased dramatically for MnO_2, MWCNT, CMK-3 with increased dosage of the radical quenching agent, whereas AND-900 and rGO-900 still attained high reaction rates of 0.004 and 0.277 min^{-1}, respectively, in the pure methanol solutions. The intrinsically different sensitivities with the radical scavenger of methanol strongly suggest the distinctive oxidation pathways on the nanocarbons.

In a recent study, we reported that single walled carbon nanotubes (SWCNTs) with a highly graphitic structure can effectively stimulate PMS to generate sulfate and hydroxyl radicals for contaminant degradation, and a characteristic nonradical oxidation was discovered upon heteroatom nitrogen doping into the sp^2-hybridized carbon network [27]. The nonradical process was also observed on N-doped rGO (Fig. S10). The interfacial interaction between PMS and the modified carbon lattice was enhanced by substitutional N-doping with positively charged carbon atoms. The N-doping gives rise to emerging nonradical pathway, in which activated PMS molecules are capable of oxidizing an organic directly on the surface of the carbocatalysts, without producing reactive radicals. This process considerably improve the effectiveness of organic removal. The same phenomenon was found in persulfate activation on CuO [26] and SWCNTs [38] for AOPs and homogeneous Gif chemistry (Fe^{II}/H_2O_2 or Fe^{III}/H_2O_2) [23] toward selective oxidation.

In this study, the radical pathways could be terminated by the high concentration of methanol. MWCNTs and CMK-3 cannot activate PMS in methanol solutions for organic removal, suggesting a pure radical-based oxidation, similar to the classic radical-based oxidation originated from PMS activation on metal-based catalysts, Co_3O_4 [27] and α-MnO_2 (Fig. S11). Moreover, emerging nonradical oxidation was exclusively discovered in the AND-900/PMS and rGO-900/PMS, as the radical shield agent (methanol) did not completely eliminate the oxidative processes. As discussed above, we suppose that the conjugated π network of highly crystallized CNTs and electron-rich kenotic groups in CMK-3 tend to directly donate electrons to PMS to produce $SO_4^{\bullet-}$ and $^{\bullet}OH$ in a redox process. However, the graphitic structures of AND-900 and rGO-900 are terminated with various defective edges derived from the thermal annealing process and removal of functional groups. The defects, especially for zigzag edges in an bordered graphene sheet, remain the sp^2 hybridization with unpaired π electrons and possess a smaller band gap at the Fermi level, compared with perfect graphene sheets with the stable and conjugated π electrons and zero-band structure [39]. The edge sites are able to confine the delocalized π system with a '*localized state*', presenting completely different electronic, magnetic, and chemical properties which may be capable of attacking radicals and dissociating small molecules such as H_2 and CH_3OH [40]. Here, the unique electronic circumstance and actively chemical state of defective edges of graphene, like outer sphere electrons of CuO, are believed to be able to weaken and dissociate the O—O bond (HO-SO_4^-) in PMS. The strong interaction between the PMS and defective sites then enable the activated PMS molecules capable of oxidizing target components directly via extracting electrons from organics without generating free radicals (as indicated in Scheme 1). This can also well support and explain the fact that the catalytic oxidation processes were greatly improved on rGO (O at% <10%) from GO (O at% >30%) as the edging defects occupied by oxygen functional groups are exposed for a better access to peroxymonosulfate. Moreover, stability tests were performed and the results can be found in Fig. S12. The used catalyst (rGO) can only show 49.1% phenol oxidation in 60 min at the second run. The poor stability of carbocatalyst was due to the change of surface chemistry. This is because the defective sites might be partially oxidized and destroyed by the reactive radicals from PMS activation in a highly oxidative environment. The change of surface chemistry was further confirmed by the XPS results which showed that the oxygen contents of deactivated rGO increased to 10.9% after the second run (Fig. S8f). Thermal treatment was applied to remove the excess oxygen functional groups and regenerate the activate site. A complete phenol removal could be achieved on the regenerated rGO sample.

Theoretical calculations were further carried out to probe PMS adsorption behaviors and cleavage of O—O bond on different carbon configurations as summarized in Table 1. Compared with a free

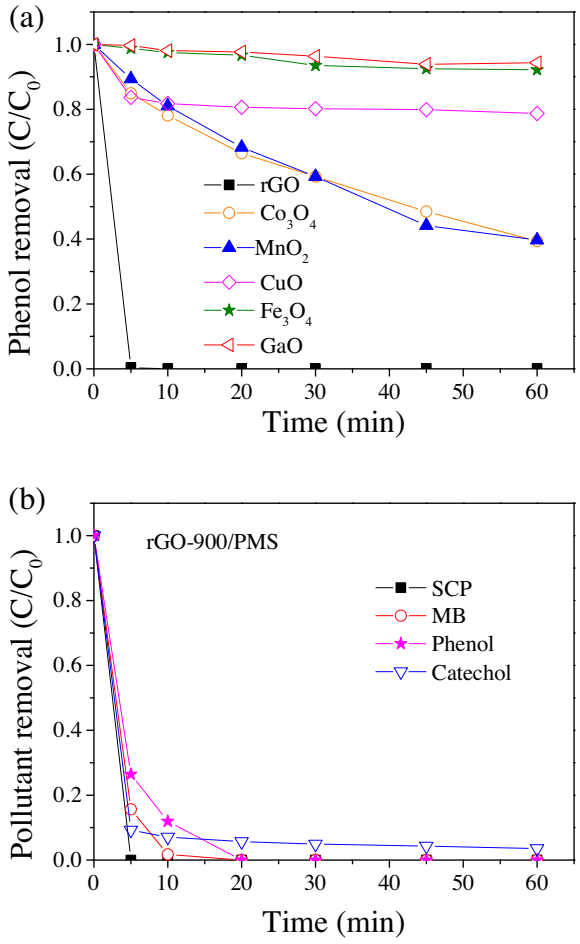

Fig. 3. (a) Comparison of metal oxides and metal-free (rGO-900) catalysts for PMS activation ($[Catalyst]_0$ = 0.1 g/L, $[PMS]_0$ = 6.5 mM, [T] = 25 °C, and $[Phenol]_0$ = 20 mg/L), (b) Catalytic oxidation of various contaminants in rGO-900/PMS. ($[Catalyst]_0$ = 0.05 g/L, $[PMS]_0$ = 6.5 mM, [T] = 25 °C, and $[Phenol]_0$ = $[Catechol]_0$ = $[SCP]_0$ = 20 mg/L or $[MB]_0$ = 10 mg/L).

Table 1
Theoretical calculations for favourable PMS (SO_4-OH) adsorption on different carbon configurations. E_{ads} represents for the adsorption energy of PMS on carbocatalysts, Q for electronic transfer between PMS and graphene, and l_{O-O} for the bond length of O—O in PMS.

Carbon structure	E_{ads} (eV)	Q (e)	l_{OO} (Å)
Free PMS molecule			1.326
SWCNT [41]	−2.05	−0.455	1.402
Zigzag edge on graphene	−2.58	−0.782	1.439
Armchair edge on graphene	−2.52	−0.725	1.454
C=O on amorphous carbon	−7.96	−1.078	Dissociated

PMS molecule without activation, the O—O bond length is obviously prolonged after adsorption on different carbocatalysts. The HO-SO_4^- directly dissociates into two parts (HO and SO_4) when PMS interacts with the carbonyl group (C=O) on amorphous carbon clusters with a mixture of sp^2- and sp^3-carbon hybridization, suggesting the generation of sulfate radicals ($SO_4^{\bullet-}$). The adsorption energy and electron-transfer tendency on single-walled carbon nanotubes (SWCNTs), with intact and graphitic sp^2-C configuration, presents a higher E_{ads} and lower Q among the carbon structures, which is in consistent with the lower activity of MWCNTs for phenol oxidation. When PMS adsorbed on the zigzag and armchair edges of pristine graphene, a relative lower E_{ads}, greater Q, and longer l_{O-O} are achieved at the same time, which contribute to the activation of a PMS molecule for nonradical oxidation without generation of free

radicals. The PMS molecules might be activated on the defective edges first and consequently oxidize the adsorbed target organics via electron conduction and H abstraction.

Furthermore, the nonradical oxidation induced by carbocatalysis is more efficient than the most universally studied metal oxides in the similar AOPs (Fig. 3a), completely overcoming the hurdles of toxic metal ion leaching. The new system is also effective for decomposition of a wide range of organics such as methylene blue (MB), 1,2-dihydroxylphenol (catechol), and a typical antibiotic sulfachloropyridazine (SCP), as indicated in Fig. 3b.

3.3. Influences of anions and background organic matters

It is always desirable for a reaction system with a good efficiency and a high selectivity. In heterogeneous AOPs, transition metal oxides such as cobalt oxide and manganese oxide with a specific exposed crystal facet and variable metal-valence states are well reported to mediate PMS to produce $SO_4^{\bullet-}$ [42,43]. In recent studies, we first reported that nanocarbons can activate persulfate to selectively produce •OH via oxidizing adjacent water molecules, other than directly producing $SO_4^{\bullet-}$, a Fenton-like process [29,41]. The emerging nonradical oxidation was also revealed in carbocatalysis/PMS and CuO/PS. To the best of our knowledge, the diverse active species and oxidation pathways present different oxidative potentials and selectivity toward target organics out of background organic matters in surface or underground waters. Therefore, it would be very interesting to investigate nonradical induced degradation of contaminants in waste water with trace amount of organics or ions in the eco-system.

In practical applications, the ions in wastewater would have pronounced influences on AOPs. The anions (such as HPO_4^{2-}, $H_2PO_4^-$, HCO_3^-, CO_3^{2-}, Cl^-, Br^-, NO_3^- etc.) can quickly react with the reactive radicals via electron exchange and then change the acidic/basic conditions in AOPs, hereby interfering the catalytic oxidation processes and efficiency. In this study, the influences of various ions on nonradical oxidation were evaluated. As indicated in Fig. 4a, $H_2PO_4^{2-}$ at a level of 5–20 mM presented a marginal effect on phenol removal. However, the introduction of HCO_3^- dramatically affected the reaction rate of phenol removal (Fig. 4b). The reaction time for complete phenol oxidation increased to 60 and 30 min, respectively, at 5 and 10 mM HCO_3^- in the solutions. However, at the concentration of 20 mM HCO_3^-, phenol was rapidly removed in just 5 min. Surprisingly, 97.2% phenol removal was achieved in 2 h when HCO_3^- alone was presented with PMS without any carbon catalyst, indicating the activation behavior of HCO_3^- for PMS. In the nonradical dominated system, the quenching effect of HPO_4^{2-} is insignificant while HCO_3^- could affect the catalytic activity of rGO-900. The versatile ions are well known to shield the reactive radicals and change the solution pH. The HPO_4^{2-} anions present acid properties while the HCO_3^- anions are basic agents, suggesting that the acidic/basic condition probably influence the nonradical reactions in PMS/rGO-900 system. It is well known that PMS activation in metal-based systems is favored under neutral and basic conditions in which OH^- can be oxidized to •OH by $SO_4^{\bullet-}$ and HSO_5^- [42]. On the contrary, at lower pHs, PMS primarily exists in the form of H_2SO_5, which is more inert to be activated for oxidation and meanwhile transition metal oxides suffer from severe metal-leaching and structural destruction [44]. Thus, the overall efficiency for organic oxidation is dramatically slowed down.

For the nonradical oxidative processes based on carbocatalysis in rGO-900/PMS, the little generated free radicals such as •OH and $SO_4^{\bullet-}$ are not critical for catalytic oxidation, thus both the radical

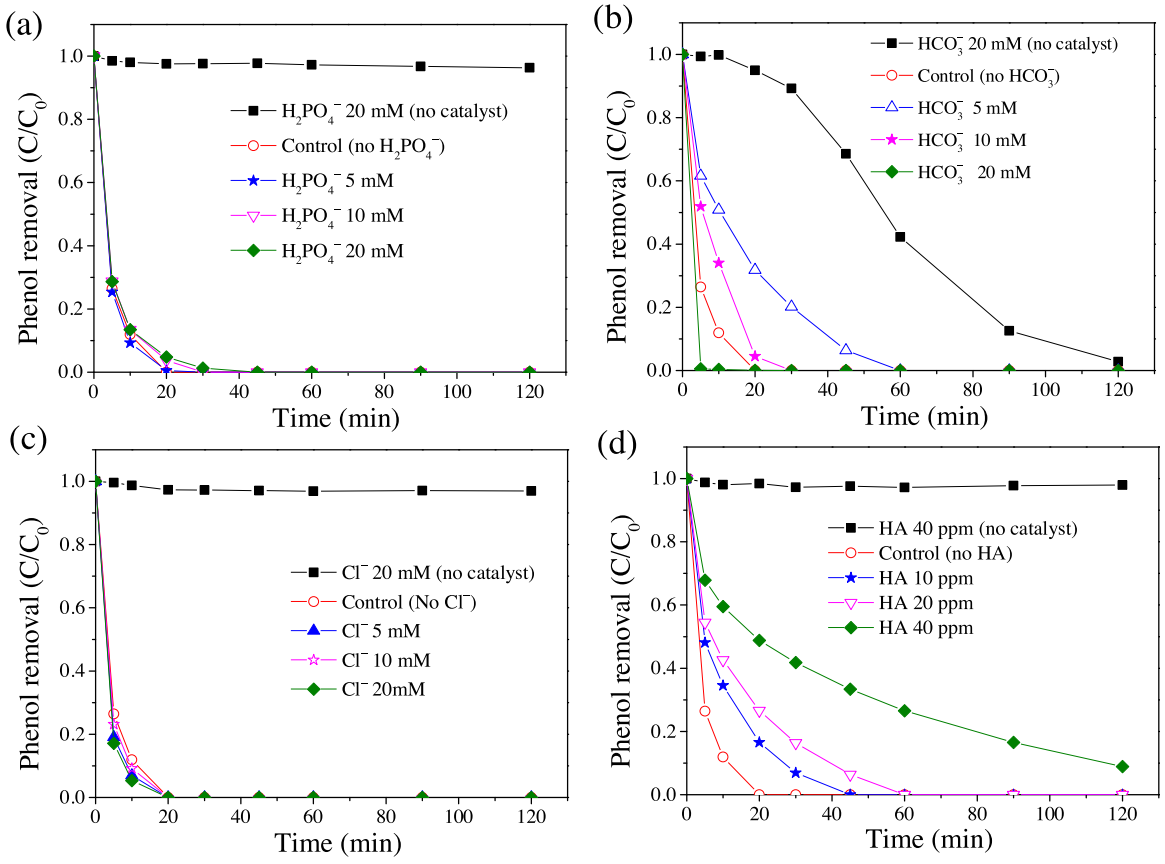

Fig. 4. Effects of radical scavengers (a) $H_2PO_4^-$, (b) HCO_3^-, (c) Cl^-, and (d) humic acid on phenol nonradical oxidation with rGO-900. ($[Catalyst]_0 = 0.05$ g/L, $[PMS]_0 = 6.5$ mM, $[T] = 25$ °C, and $[Phenol]_0 = 20$ mg/L).

scavengers and pH should have a minor effect on PMS activation, just like $H_2PO_4^{2-}$. However, the reaction rate constants (Fig. S13) decreased from 0.21 to 0.05 and 0.15 min^{-1} at 5 and 10 mM HCO_3^-, respectively, while it increased to 0.35 min^{-1} at 20 mM HCO_3^-. We suppose that a minor amount of HCO_3^- was able to tune the acid property and surface charge of rGO, giving rise to a decreased degradation efficiency. When excessive HCO_3^- (20 mM) was presented, the solution was adjusted to a mild basic buffer solution (pH 8) which facilitates the dissociation of PMS molecules and the PMS turned into SO_5^{2-} which is more easily to be activated in heterogeneously oxidative reactions [45]. This is further supported by the fact that HCO_3^- (20 mM)/PMS alone without any carbocatalyst can still achieve efficient phenol removal. The effect of pH is indicated in Fig. S14. Complete phenol removal can be achieved in less than 20 min within a wide pH range (2.1 − 11.0) in rGO-900/PMS, and complete phenol removal was quickly attained in just 5 min under a highly basic environment (pH 11.0) even without the catalysts, implying that PMS ($pK_{a1} < 0$; $pK_{a2} = 9.88$) will become a strong oxidant (SO_5^{2-}) in the basic condition.

Sulfate radicals generated from PMS or PS in AOPs have the advantages of possessing a higher oxidative potential ($SO_4^{\bullet-}$, 2.5–3.1 V) and a better selectivity toward target aromatic compounds than the non-selective hydroxyl radicals (•OH, 1.8–2.7 V), however, $SO_4^{\bullet-}$ tends to be rapidly scavenged by halogen ions [14,26,46]. Hydroxyl radicals also suffer from the shield of Cl^- in strong acid solutions [47]. The halogen radicals, such as $Cl^{\bullet-}$, $Cl_2^{\bullet-}$ and $Br^{\bullet-}$, present lower oxidative potentials for organic mineralization and can convert phenolics into chlorophenols which are more difficult to be degraded [47,48]. The drawbacks of $SO_4^{\bullet-}$ hinder the application of PMS and PS in processing domestic sewage and industry wastewaters which usually contain high salinity. The effect of chloride was then estimated in the rGO-900/PMS system. As indicated in Fig. 4c, increasing Cl^- concentration from 5–20 mM did not affect the phenol removal efficiency, suggesting that sulfate radicals are not the active species accounting for the oxidation of organics in the rGO-900/PMS system and the nonradical pathway plays a crucial role in phenol decomposition. Unlike $SO_4^{\bullet-}$, the nonradical oxidation was reported not capable of oxidizing chloride ions into chlorine radicals [26]. Therefore, the nonradical pathway can attain effective mineralization of contaminants without the generation of more hazardous chlorinated products. It can be then deduced that the emerging nonradical processes can be adapted to a wide pH range and demonstrate superb resistance to various radical scavengers, which are different from the radical based processes in MWCNTs/PMS and MnO_2/PMS systems shown in Fig. S15.

The versatile natural organic matters (NOMs) in the natural eco-system can undergo competitive reactions with the reactive species in AOPs and then minimize the decomposition efficiency towards target components, especially for •OH dominated system [42]. On the other hand, sole phenol or quinone molecules and semi-quinone groups in NOMs are also reported to be able to initiate PMS and persulfate to evolve •OH and $SO_4^{\bullet-}$ for organic degradation via a self-redox cycle [45,49,50]. Herein, the implication of a typical NOM, humic acid (HA), was taken into account in the nonradical oxidation. Fig. 4d suggests that HA alone cannot activate PMS for phenol oxidation. The phenol removal rate decreased gradually with the addition of HA from 10 to 40 mg L^{-1}, yet a better and selective phenol oxidation at 91.2% was still achieved in coexistence of excess HA (40 mg L^{-1}), compared with 20.4% and 66.1% phenol removal on SWCNT and MnO_2. We suppose that humic acid and its mineralized intermediates not only compete with phenol for reacting with PMS via nonradical pathway (reflected by the rapid de-colorization of the brown mixture solution, Fig. S16), but also block the active sites with various oxygen groups via strong π-π stacking which prohibit the interaction of the carbocatalysts with PMS and phenol.

4. Conclusions

In summary, various nanocarbons were employed as efficient carbocatalysts for catalytic organic oxidation with PMS. The carbocatalysts present intrinsically differing sensitivities to high dosage of radical scavengers, revealing that diverse active sites may play different roles in PMS activation. The kenotic groups and sp^2 hybridized carbon lattice can donate electrons to PMS to produce sulfate and hydroxyl radicals, whereas the defective edges on annealed nanodiamond and rGO give rise to an emerging nonradical pathway. The nonradical oxidation was effective in a wide pH range, resistant to various anions, meanwhile presenting a better selectivity to target contaminants with the presence of background organic matters. This study proposes a novel and effective oxidation strategy and enables new insights into heterogeneous PMS activation in aqueous and nonaqueous solutions with the state-of-the art carbocatalysis.

Acknowledgements

This work is financially supported by Australian Research Council under project No. DP130101319. H.S. is grateful of Curtin Research Fellowship.

Appendix A. Supplementary data

Supplementary data associated with this article can be found, in the online version, at http://dx.doi.org/10.1016/j.apcatb.2016.01.059.

References

[1] X.B. Wang, Y.L. Qin, L.H. Zhu, H.Q. Tang, Environ. Sci. Technol. 49 (2015) 6855–6864.
[2] T. Zhang, H.B. Zhu, J.P. Croue, Environ. Sci. Technol. 47 (2013) 2784–2791.
[3] V.J.P. Vilar, F.C. Moreira, A.C.C. Ferreira, M.A. Sousa, C. Goncalves, M.F. Alpendurada, R.A.R. Boaventura, Water Res. 46 (2012) 4599–4613.
[4] A.K. Verma, R.R. Dash, P. Bhunia, J. Environ. Manage. 93 (2012) 154–168.
[5] J.A. Zazo, J.A. Casas, A.F. Mohedano, M.A. Gilarranz, J.J. Rodriguez, Environ. Sci. Technol. 39 (2005) 9295–9302.
[6] Y.W. Kang, K.Y. Hwang, Water Res. 34 (2000) 2786–2790.
[7] S. Navalon, R. Martin, M. Alvaro, H. Garcia, Angew. Chem. Int. Ed. 49 (2010) 8403–8407.
[8] Y.X. Wang, H.Q. Sun, X.G. Duan, H.M. Ang, M.O. Tade, S.B. Wang, Appl. Catal. B 172 (2015) 73–81.
[9] X.W. Liu, X.F. Sun, D.B. Li, W.W. Li, Y.X. Huang, G.P. Sheng, H.Q. Yu, Water Res. 46 (2012) 4371–4378.
[10] G.P. Anipsitakis, D.D. Dionysiou, M.A. Gonzalez, Environ. Sci. Technol. 40 (2006) 1000–1007.
[11] P. Neta, V. Madhavan, H. Zemel, R.W. Fessenden, J. Am. Chem. Soc. 99 (1977) 163–164.
[12] G.P. Anipsitakis, D.D. Dionysiou, Environ. Sci. Technol. 38 (2004) 3705–3712.
[13] J. Zou, J. Ma, L.W. Chen, X.C. Li, Y.H. Guan, P.C. Xie, C. Pan, Environ. Sci. Technol. 47 (2013) 11685–11691.
[14] M.G. Antoniou, A.A. de la Cruz, D.D. Dionysiou, Appl. Catal. B 96 (2010) 290–298.
[15] R.O.C. Norman, P.M. Storey, P.R. West, J. Chem. Soc. B (1970) 1087–1095.
[16] G.P. Anipsitakis, D.D. Dionysiou, Environ. Sci. Technol. 37 (2003) 4790–4797.
[17] E. Saputra, S. Muhammad, H.Q. Sun, H.M. Ang, M.O. Tade, S.B. Wang, Appl. Catal. B 142 (2013) 729–735.
[18] Q.J. Yang, H. Choi, D.D. Dionysiou, Appl. Catal. B 74 (2007) 170–178.
[19] H.Q. Sun, S.Z. Liu, G.L. Zhou, H.M. Ang, M.O. Tade, S.B. Wang, ACS Appl. Mater. Interfaces 4 (2012) 5466–5471.
[20] S. Indrawirawan, H. Sun, X. Duan, S. Wang, Appl. Catal. B 179 (2015) 352–362.
[21] S. Navalon, A. Dhakshinamoorthy, M. Alvaro, H. Garcia, Chem. Rev. 114 (2014) 6179–6212.
[22] C.L. Su, K.P. Loh, Acc. Chem. Res. 46 (2013) 2275–2285.
[23] F. Gozzo, J. Mol. Catal. A 171 (2001) 1–22.
[24] F. Shi, M.K. Tse, Z.P. Li, M. Beller, Chem. Eur. J. 14 (2008) 8793–8797.
[25] T. Zhang, W.W. Li, J.P. Croue, Appl. Catal. B 121 (2012) 88–94.
[26] T. Zhang, Y. Chen, Y. Wang, J. Le Roux, Y. Yang, J.-P. Croué, Environ. Sci. Technol. 48 (2014) 5868–5875.

[27] X.G. Duan, H.Q. Sun, Y.X. Wang, J. Kang, S.B. Wang, ACS Catal. 5 (2015) 553–559.
[28] W.S. Hummers, R.E. Offeman, Preparation of graphitic oxide, J. Am. Chem. Soc. 80 (1958) 1339.
[29] X.G. Duan, H.Q. Sun, J. Kang, Y.X. Wang, S. Indrawirawan, S.B. Wang, ACS Catal. 5 (2015) 4629–4636.
[30] H.Q. Sun, Y.X. Wang, S.Z. Liu, L. Ge, L. Wang, Z.H. Zhu, S.B. Wang, Chem. Commun. 49 (2013) 9914–9916.
[31] N. Keller, N.I. Maksimova, V.V. Roddatis, M. Schur, G. Mestl, Y.V. Butenko, V.L. Kuznetsov, R. Schlogl, Angew. Chem. Int. Ed. 41 (2002) 1885-+.
[32] J.A. Zhang, D.S. Su, R. Blume, R. Schlogl, R. Wang, X.G. Yang, A. Gajovic, Angew. Chem. Int. Ed. 49 (2010) 8640–8644.
[33] X.G. Duan, Z.M. Ao, H.Q. Sun, S. Indrawirawan, Y.X. Wang, J. Kang, F.L. Liang, Z.H. Zhu, S.B. Wang, ACS Appl. Mater. Interfaces 7 (2015) 4169–4178.
[34] H.Q. Sun, C. Kwan, A. Suvorova, H.M. Ang, M.O. Tade, S.B. Wang, Appl. Catal. B 154 (2014) 134–141.
[35] Y.M. Lin, D.S. Su, ACS Nano 8 (2014) 7823–7833.
[36] W.C. Peng, S.Z. Liu, H.Q. Sun, Y.J. Yao, L.J. Zhi, S.B. Wang, J. Mater. Chem. A 1 (2013) 5854–5859.
[37] C.J. Liang, H.W. Su, Ind. Eng. Chem. Res. 48 (2009) 5558–5562.
[38] H. Lee, H.J. Lee, J. Jeong, J. Lee, N.B. Park, C. Lee, Chem. Eng. J. 266 (2015) 28–33.
[39] K. Nakada, M. Fujita, G. Dresselhaus, M.S. Dresselhaus, Phys. Rev. B 54 (1996) 17954–17961.
[40] D.E. Jiang, B.G. Sumpter, S. Dai, J. Chem. Phys. 126 (2007) 134701.
[41] X.G. Duan, Z.M. Ao, H.Q. Sun, L. Zhou, G.X. Wang, S.B. Wang, Chem. Commun. 51 (2015) 15249–15252.
[42] P. Hu, M. Long, Appl. Catal. B 181 (2016) 103–117.
[43] E. Saputra, S. Muhammad, H.Q. Sun, H.M. Ang, M.O. Tade, S.B. Wang, Environ. Sci. Technol. 47 (2013) 5882–5887.
[44] Y.M. Ren, L.Q. Lin, J. Ma, J. Yang, J. Feng, Z.J. Fan, Appl. Catal. B 165 (2015) 572–578.
[45] Y.H. Guan, J. Ma, Y.M. Ren, Y.L. Liu, J.Y. Xiao, L.Q. Lin, C. Zhang, Water Res. 47 (2013) 5431–5438.
[46] J.E. Grebel, J.J. Pignatello, W.A. Mitch, Environ. Sci. Technol. 44 (2010) 6822–6828.
[47] Y. Yang, J.J. Pignatello, J. Ma, W.A. Mitch, Environ. Sci. Technol. 48 (2014) 2344–2351.
[48] Y. Yang, J. Jiang, X.L. Lu, J. Ma, Y.Z. Liu, Environ. Sci. Technol. 49 (2015) 7330–7339.
[49] M. Ahmad, A.L. Teel, R.J. Watts, Environ. Sci. Technol. 47 (2013) 5864–5871.
[50] G.D. Fang, J. Gao, D.D. Dionysiou, C. Liu, D.M. Zhou, Environ. Sci. Technol. 47 (2013) 4605–4611.